Sine Resistance Network-Based Motion Planning Approach for Autonomous Electric Vehicles in Dynamic Environments

Tenglong Huang, Huihui Pan, Weichao Sun, *Senior Member, IEEE*, and Huijun Gao, *Fellow, IEEE*

***Abstract*— This article proposes a motion planning approach for autonomous electric vehicles to generate an appropriate planned path according to the time-varying surrounding information. This approach utilizes the proposed novel sine resistance network to mesh the road with the aim of improving the planned path smoothness, which has the capability of generating a continuous-curvature planned path that contributes to tracking and reducing the jerkiness. Meanwhile, considering that the classical artificial potential field (APF) method is only suitable for the static scenarios, a bias oval APF is constructed to predict the change of relative distance between the ego vehicle and each obstacle by taking the speed information into account. The proposed planning approach can ensure that the planned path is collision-free in dynamic environments and the generated path is smooth simultaneously. Cosimulation results in CarSim and MATLAB/Simulink are provided to prove the advantage and feasibility of the proposed motion planning approach for autonomous electric vehicles.**

***Index Terms*— Autonomous electric vehicles, bias oval artificial potential field, collision free, motion planning, sine resistance network.**

I. Introduction

NUMEROUS collision accidents are caused by human error and the traffic is getting more and more congested [1]. Autonomous electric vehicles contribute to reducing traffic accidents and relieving traffic congestion, and thus, they have attracted considerable interest from industry and academic researchers in the last decades. Relevant research in academia emerged from the PROMETHEUS project, and then, DARPA challenges brought about prosperity and rapid development in this field [2]. The advanced technology for autonomous electric vehicles has been one of the most popular and promising fields of research in recent years [3], [4].

A typical autonomous electric vehicle is composed of three modules: perception module, planning module, and control module. Based on the surrounding information obtained from the perception module, the motion planning module generates the planned behavior and path, and the control module is utilized to track the planned motion. The motion planning module plays a vital role in autonomous electric vehicles and is considered as the "brain" of the autonomous vehicle. As the fundamental and essential module of autonomous vehicles, there have been numerous research results about planning. In comparison to combining path planning and velocity planning, generating the planned path and velocity separately can reduce computational consumption [5]. Meanwhile, traditional path planning has been studied in a considerable amount of literature. To mention some research efforts, the geometry-based method is developed in [6], where path generation is based on the Voronoi cell algorithm with high computational efficiency. The grid-based methods are proposed for generating the shortest path such as Dijkstra's algorithm [7] and A* algorithm [8]. To find a collision-free planned path, the lattice and network-based algorithm are investigated in [9], which can avoid obstacles effectively. Note that the artificial potential field (APF) method studied in [10]–[12] has already drawn increased attention due to the ability to ensure collision-free. Artificial intelligence (AI)-based methods have made significant progress, such as convolutional neural network (CNN) algorithm in [13] and Q-learning algorithm in [14]. The CNN algorithm can follow the lane without planning and control, and the Q-learning algorithm is able to cope with different road geometries. Nevertheless, many algorithms are derived from the field of robotics, and the generated trajectories may have discontinuous curvature, which is not suitable for autonomous vehicle motion characteristics, such as grid-based methods. Meanwhile, most planning algorithms treat obstacles as static, which are difficult to deal with dynamic scenes, such as the traditional APF method. Moreover, some planning algorithms require massive data for training or are difficult to use in actual scenarios, such as algorithms based on CNN and reinforcement learning. Thus, it is essential to explore

Manuscript received November 22, 2021; revised January 30, 2022; accepted February 4, 2022. Date of publication February 16, 2022; date of current version April 20, 2022. This work was supported in part by the National Natural Science Foundation of China under Grant U1964201 and Grant 62173108, in part by the Major Scientific and Technological Special Project of Heilongjiang Province under Grant 2021ZX05A01, in part by XPLORE PRIZE, and in part by the Fundamental Research Funds for the Central Universities. *(Corresponding authors: Huihui Pan; Huijun Gao.)*

Tenglong Huang is with the Research Institute of Intelligent Control and Systems, Harbin Institute of Technology, Harbin 150001, China, and also with Ningbo Institute of Intelligent Equipment Technology Company Ltd., Ningbo 315200, China (e-mail: huangtenglong@hit.edu.cn).

Huihui Pan is with the Research Institute of Intelligent Control and Systems, Harbin Institute of Technology, Harbin 150001, China, and also with the Robot Innovation Center, Harbin Institute of Technology, Harbin 150001, China (e-mail: huihuipan@hit.edu.cn).

Weichao Sun is with the Research Institute of Intelligent Control and Systems, Harbin Institute of Technology, Harbin 150001, China (e-mail: w.sun@hit.edu.cn).

Huijun Gao is with the Research Institute of Intelligent Control and Systems, Harbin Institute of Technology, Harbin 150001, China, and also with the Department of Mathematics and Theories, Peng Cheng Laboratory, Shenzhen 518055, China (e-mail: hjgao@hit.edu.cn).

Digital Object Identifier 10.1109/TTE.2022.3151852

a collision-free planning algorithm suitable for autonomous vehicles in dynamic scenarios. The detailed limitations and advantages of these methods are summarized in [15]. Each algorithm has high performance in the corresponding applicable scenarios and leaves room for improvement at the same time.

At present, the development of autonomous electric vehicles is mainly limited by the planning module [16]. How to make an appropriate decision and generate a smooth trajectory based on the dynamic surrounding information is the primary challenge, which further enhances the research significance of motion planning. Note that an interesting and promising path planning approach based on the square impedance network is presented in [9] for the first time. Nevertheless, autonomous vehicles with nonholonomic characteristics cannot follow the planned rectangle path. To solve this problem, a novel diamond grid is presented in [17], which handles this problem successfully; however, the curvature of the planned path for the ego vehicle is discontinuous obviously. The network-based approaches can reflect the surrounding environment intuitively by changing the resistance in each branch, which shows the great potential for motion planning in traffic. Inspired by this characteristic, the novel sine resistance network (SRN) is proposed in this article. Meanwhile, compared with the other planning algorithms, the APF method has the inherent advantage of avoiding obstacles. However, the classic APF method only applies to static scenarios, and the vehicle needs to cope with the dynamic scenarios in real-world scenarios. Moreover, some pioneering APF-based work has been proposed for mobile robotics, such as [18]–[23]. However, the planned path generated according to the potential field gradient may not be well suitable for electric vehicles. Therefore, a modified version of the APF method is proposed to predict the change of relative distance between the ego vehicle and each obstacle in the dynamic environment by considering the speed information, and the method can generate a collision-free path simultaneously in this article. To achieve the desired planning performance and verify the planning algorithm, an excellent trajectory tracking method is essential. A high amount of tracking control approaches can be utilized to follow the planned trajectory, which can be provided in the comprehensive reviews [24], [25]. For the sake of safety and comfort, the inputs, states, and outputs of autonomous vehicles should satisfy the corresponding constraints. Thus, a controller based on model predictive control (MPC) is designed to handle the multiple constraints in this article. As discussed above, motion planning is the major challenge in the autonomous electric vehicles field, which motivates the study in this article.

This article focuses on the problem of local path planning for autonomous electric vehicles. A novel motion planning and tracking architecture is proposed for autonomous vehicles to balance these performance criteria. The contributions of this article can be listed as follows.

1) The sine grid is presented for the first time to construct a novel SRN. The proposed novel sine grid avoids the curvature discontinuity for the traditional network-based methods. The curvature of the planned path is continuous, and thus, the path smoothness and overall performance are improved significantly.
2) The bias oval artificial potential field (BOAPF) is generated by taking the velocity information into account. The modified APF method can cope with the dynamic surrounding rather than only be applicable in the static surrounding.
3) Different driver styles can be selected with different conservative coefficients or sine grid structures by the proposed method in this article. Meanwhile, the performance comparison has been performed between the state-of-the-art (SOTA) network-based algorithm named diamond resistance network (DRN) and the proposed algorithm.

II. Overall Structure of the Proposed Framework

The common objective of autonomous electric vehicles is to implement an algorithm that can guarantee that the subject vehicle is collision-free at each time instance. A schematic representation of the overall framework for the proposed algorithm to achieve this goal can be seen in Fig. 1.

The motion planning problem is solved by utilizing the combination of SRN and BOAPF in this article. The road is meshed by an SRN that is designed meticulously with the aim of improving planned path smoothness. Based on the road and surrounding obstacles information, the BOAPF can be constructed. Compute the resistance value of each edge for the SRN according to the superposed APF. The current for each edge of SRN can be generated by adding the virtual voltage source. Choose the maximum outward current to determine the planned path. In this context, the motion planning is accomplished. Subsequently, the path-tracking problem is converted into an optimization problem with the constraints based on the single-track vehicle model.

The overall structure describes the main components of the proposed approach, which consists of two modules: the motion planning module to generate a collision-free path and behavior and the path-tracking module based on MPC to follow the planned path. To verify the feasibility of the proposed algorithm, four typical scenarios are cosimulated in CarSim and MATLAB/Simulink.

III. Main Results

In this section, a method is presented to address the motion planning problem for autonomous electric vehicles, which generates a novel SRN to mesh the road for the first time and constructs the BOAPF by considering the velocity information of the vehicles to cope with the dynamic environments. Finally, a planned collision-free path is obtained via a combination of the SRN and BOAPF.

A. SRN Generation

Due to the curvature discontinuity appeared in the traditional grid-based path planning algorithm mentioned above, performance may suffer degradation or even the algorithm is not feasible. To mitigate this issue, a novel SRN is introduced to generate a planned collision-free smooth path based on the designed sine grid, as shown in Fig. 2.

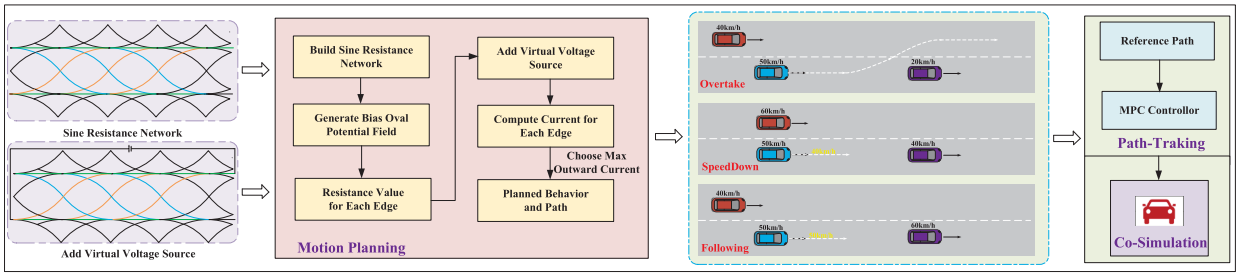

Fig. 1. Overall structure of the proposed approach.

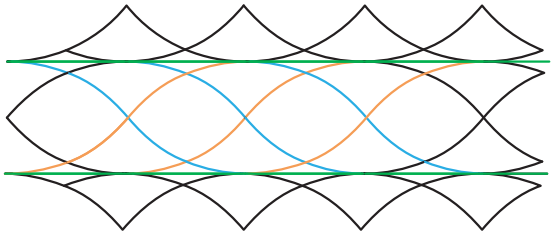

Fig. 2. Proposed SRN.

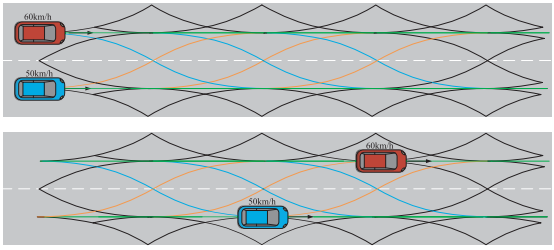

Fig. 3. SRN on straight road with two lanes.

It is noteworthy that various driver styles can be selected by designing different structures of the SRN. One of the most crucial factors to choose the driver styles is the longitudinal length of the sine grid for SRN. Compared to an aggressive driver, the conservative driver needs a longer distance to change into the adjacent lane. Moreover, the number of sine grids for the SRN denotes the prediction distance for the ego vehicle. Finally, the expected driver style can be chosen by regulating the parameters to generate the corresponding structure of the SRN.

To further demonstrate the operating principle of the SRN, a typical scenario is shown in Fig. 3, where the road is covered with the presented SRN, and the green lines locate at the centerlines of the two lanes. Furthermore, the amplitude of the sinusoidal function is set according to the width of the road, and the period of the sinusoidal function is adjusted according to the different driver styles.

Remark 1: The proposed SRN inspired by the notable and promising path planning approaches [9], [17], [26] is used to generate a continuous-curvature planned path and improve path smoothness. The square impedance network presented in [9] can generate a short planned path effectively, but the nonholonomic characteristic may cause the vehicles unable to drive in any direction to follow the planned rectangle path. Huang *et al.* [17] developed a diamond grid, which solves this problem successfully; however, the curvature of the planned path for the ego vehicle is discontinuous, which leaves room for improvement. In contrast, the proposed SRN used to mesh the road is capable of generating a continuous-curvature path. As a result, the proposed SRN in this section improves the planned path smoothness significantly compared to the square impedance network [9] and the diamond grid [17].

B. Bias Oval Artificial Potential Field

Different from the classical method to construct the APF which only contains the APF of the obstacles in [10], the proposed BOAPF considers the information of the road and velocity information of obstacles. In this section, the total superposed APF is composed of the repulsive potential fields of the obstacles and the APF of the road. Moreover, considering that the outline of the vehicle is generally rectangular, the potential field of the vehicle is established as an ellipse instead of a circle.

1) APF of the Road: Considering that the risk coefficients for the boundary of the road are largest for vehicles, the risk coefficients for centerlines of two lanes are smallest, and the risk coefficient for the centerline of the road is situated between the two. A trigonometric function with a small amplitude is utilized to generate the APF of the region between the two centerlines of lanes. In contrast, exponential functions with a large amplitude are designed to construct the APF of the other region due to the surge of riskiness.

The mathematical expression of the APF for the road can be described as

$$P_R(X,Y)=\begin{cases}\alpha_1\left(e^{|X-X_l|}-1\right), & X\le\dfrac{W}{4}\\ \alpha_2\left(\sin\left(\dfrac{2(X-X_l)}{W}\right)\right), & \dfrac{W}{4}<X<\dfrac{3W}{4}\\ \alpha_1\left(e^{|X-X_u|}-1\right), & X\ge\dfrac{3W}{4}\end{cases}\quad(1)$$

where $\alpha_1=0.5$ and $\alpha_2=0.5$ are the gain coefficients of the APF for the road, W is the lateral width of the road, X_u and X_l are the lateral position of centerlines for the upper and lower lanes, respectively, X and Y denote the lateral and longitudinal coordinates, and $P_R(X,Y)$ denotes the APF of the road at the coordinate (X,Y).

The 3-D diagrammatic representation of the function (1) and the corresponding contour map are shown in Fig. 4(a) and (b), respectively. Not only the constructed exponential function value increases from the road centerline to edge but also

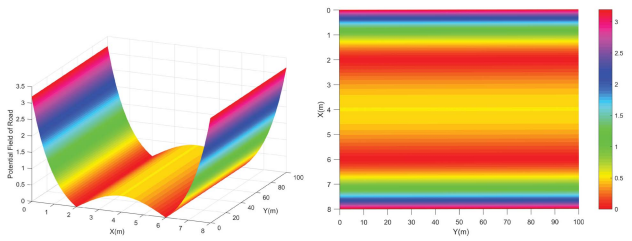

(a) (b)

Fig. 4. Detailed information of the potential field for road. (a) Potential field of road. (b) Corresponding contour map.

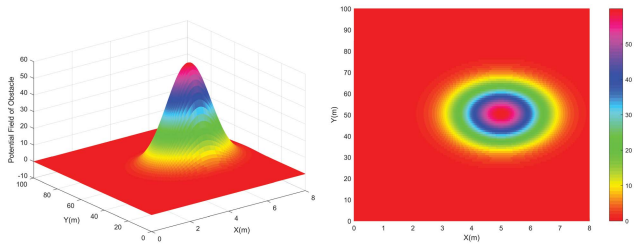

(a) (b)

Fig. 5. Detailed information of the potential field for obstacle. (a) Potential field of obstacle. (b) Corresponding contour map.

its derivative increases accordingly, which could reflect that the road risk changes reasonably. As shown in Fig. 4(b), a bird's-eye view of the road potential field is provided in the corresponding contour map where the centerline gets the minimum function value. This means that the ego vehicle always attempts to keep in the centerline without consideration of obstacles.

2) APF of Obstacle: Unlike the traditional APF method using a circular APF, that is, the values of the APF at the same distance from the center of the obstacle are equal. Considering that vehicles are in general rectangular, the elliptic potential field is used to construct the APF of obstacle in this section.

Therefore, the mathematical expression of the elliptic APF for obstacle can be written as

$$P_O(X,Y)=\beta\left(e^{-\frac{1}{2}\left(\frac{(X-X_o)^2}{\gamma_1^2}+\frac{(Y-Y_o)^2}{\gamma_2^2}\right)}-P_C\right) \tag{2}$$

where $\beta=60$ is the gain coefficient of the APF for obstacle, X_o and Y_o denote the coordinate of the obstacle, $\gamma_1=1$ and $\gamma_2=9$ are the form parameters of the APF for obstacle, $P_C=0.0001$ is a minimal positive constant, and $P_O(X,Y)$ denotes the APF of the obstacle at the coordinate (X,Y).

The 3-D diagrammatic representation of the function (2) and the corresponding contour map are shown in Fig. 5.

3) Total Superposed Potential Field: The total superposed potential field (TSPF) is the sum of the potential field of the road and potential fields of obstacles

$$P_T=P_R+\sum_{i=1}^{n}P_{O_i} \tag{3}$$

where i denotes the ith obstacle, P_{O_i} denotes the APF of the ith obstacle, and P_T denotes the TSPF.

Compared to the traditional APF method that contains nothing but static environment information, this article takes the velocity information into consideration by adjusting the APF function of the obstacle to cope with the dynamic and time-varying surrounding environment.

Different from the primitive TSPF function P_T, the presented BOAPF can be expressed as follows:

$$P_{\mathrm{BO}_i}(X,Y)=\beta\left(e^{-\frac{1}{2}\left(\frac{(X-X_o)^2}{\gamma_1^2}+\frac{(Y-Y_o+\mathrm{Bias}_i)^2}{\gamma_2^2}\right)}-P_C\right) \tag{4}$$

where $P_{\mathrm{BO}_i}(X,Y)$ denotes the APF of the ith obstacle, which considers the velocity information.

Bias can be computed by considering the speed difference as follows:

$$\mathrm{Bias}_i=\lambda\left(V_{O_i}-V_{\mathrm{Ego}}\right) \tag{5}$$

where Bias_i denotes the offset value of the ith obstacle, V_{Ego} is the longitudinal velocity of the ego vehicle in (X_{Ego} and Y_{Ego}), and V_{O_i} is the longitudinal velocity of the ith obstacle. $\lambda=0.8$ denotes the conservative coefficient, and the desired diver style can be selected by regulating the parameter λ.

Hence, the BOAPF can be calculated as follows:

$$P_{\mathrm{BOAPF}}=P_R+\sum_{i=1}^{n}P_{\mathrm{BO}_i}. \tag{6}$$

Remark 2: In comparison to [10], we also further consider the velocity information of the ego vehicle and obstacles to construct the BOAPF. The APF of the vehicle is constructed as an ellipse instead of a circle because the outline of the vehicle is rectangular. Meanwhile, the BOAPF generated is utilized to assign the resistance value of each edge in the SRN. Furthermore, the resistance provides a basis for generating the current of each edge for SRN to obtain the planned path.

Remark 3: We can choose the desired driver style by the proposed method in this article. The driver style can be chosen by adjusting the conservative coefficient λ or the period of the sinusoidal function for the SRN. A larger conservative coefficient λ means that the driver is more cautious about speed differences, indicating a more conservative driver style. In addition, a more conservative driver style can be selected by enlarging the period of the sinusoidal function for the SRN.

C. Path Planning via SRN

In this section, the SRN is designed to model the environment because searching a shorter and collision-free path is similar to the characteristic that current flows along the edge with lower resistance in the circuit. By computing the current of each edge for the resistance network, the planned path can be generated.

The detailed structure of the proposed SRN is diagramed in Fig. 6. The resistance of each edge for SRN is omitted to illustrate the principle of planned path generation more intuitively. The road with double lanes is utilized to explain the principle of path generation as an example. Naturally, the SRN is easily extended to other scenarios with structured roads.

Assign the resistance of each branch according to the value of the BOAPF. Then, the current of each branch can be

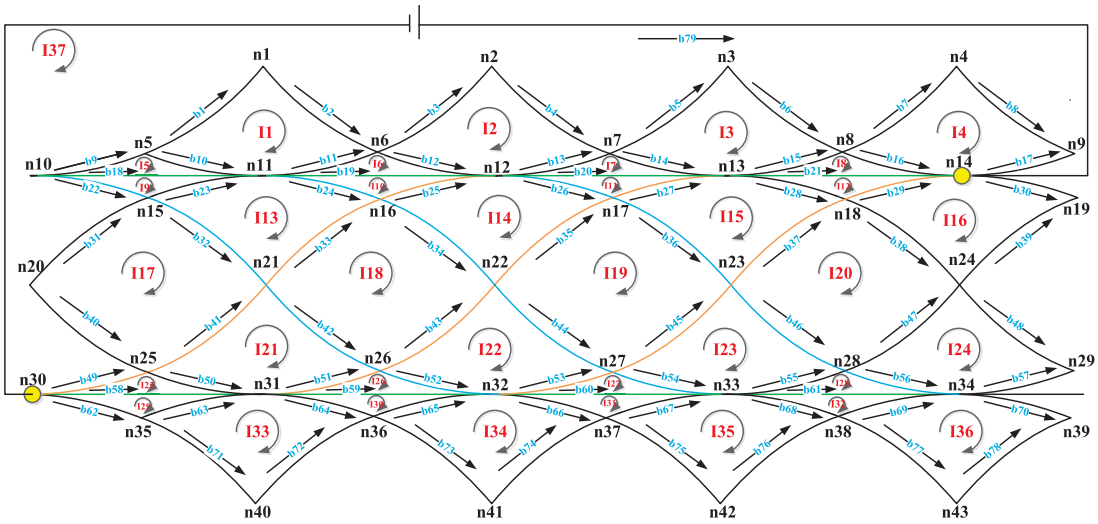

Fig. 6. Detailed structure of the proposed SRN.

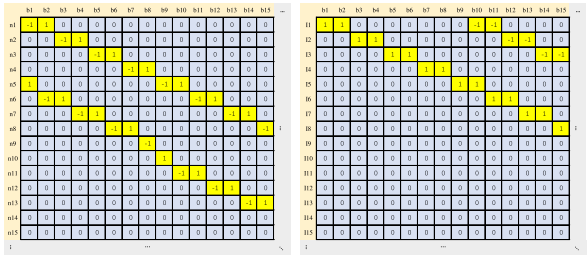

(a) (b)

Fig. 7. Relationship matrix Q_n and H generation. (a) Q_n matrix generation. (b) H matrix generation.

calculated by adding a virtual voltage source as shown in Fig. 6, where the principle to generate the current is based on the Kirchhoff circuit laws. A resistance matrix R determined by BOAPF can be written as follows:

$$R = \text{diag}[R_1, R_2, \ldots, R_i, \ldots, R_b] \tag{7}$$

where R_i indicates the resistance of ith branch and b denotes the number of the branches.

As shown in Fig. 6, the number of nodes and grids is denoted as n and g, respectively. These numbers satisfy equation $b = g + n - 1$ [9]. As shown in Fig. 7(a), an $n \times b$ dimensional matrix Q_n is computed to indicate the relationship between branches and nodes, where -1 and $+1$ indicate the hypothesized direction of current flowing into or out the corresponding node, respectively, and 0 indicates the disconnection between the branch and the corresponding node. Q can be computed by deleting any row from Q_n. Moreover, a $(b-n+1)\times b$ dimensional matrix H, as shown in Fig. 7(b), is calculated to indicate the relationship between branches and grids, where $+1$ indicates that the assumed direction of current for the branch is the same as the assumed current direction of the corresponding grid. The voltage vector V and the current vector I can be written as follows:

$$V_{b\times 1} = [V_1, V_2, \ldots, V_i, \ldots, V_b]^T \tag{8}$$

$$I_{b\times 1} = [I_1, I_2 \ldots, I_i, \ldots, I_b]^T. \tag{9}$$

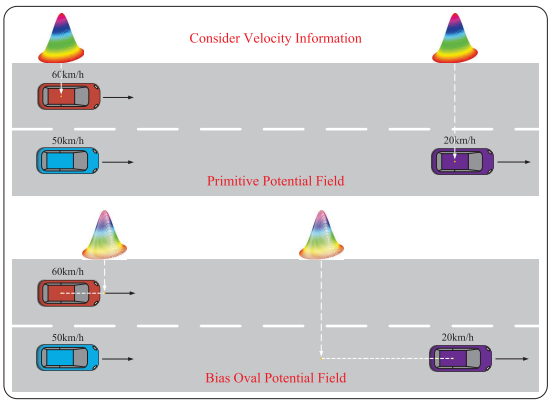

Fig. 8. Schematic of a simple scenario.

Based on the Kirchhoff circuit laws, the following equations hold.

$$Q_n I_{b\times 1} = 0_{n\times 1} \tag{10}$$

$$H_{g\times b} V_{b\times 1} = 0_{g\times 1}. \tag{11}$$

Therefore, the following equation is established by adding virtual voltage source V_s:

$$I_{b\times 1} = \left[Q_{(n-1)\times b};\ \left(H_{g\times b} R_{b\times b}\right)\right]^T \backslash \left[0_{(n-1)\times b};\ H_{g\times b}\right]\left[0_{1\times(b-1)},\ V_s\right]^T \tag{12}$$

where $V_s = 50(v)$ is chosen in this article and matrix $I_{b\times 1}$ denotes the current of the corresponding branch in the SRN, as shown in Fig. 6. From the starting node to the target node, choosing the direction of maximum outward current is to generate the planned collision-free path, where the approach is to compare the currents at each node as [27] did.

D. Considering Dynamic Environment Information

This section explains the principle of generating the planned behavior and path by considering the dynamic environment information. The velocity information is taken into consideration by moving the primitive potential field. According to the

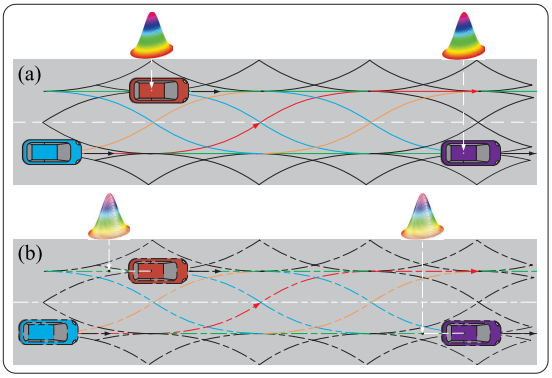

Fig. 9. Schematic of overtake scenario.

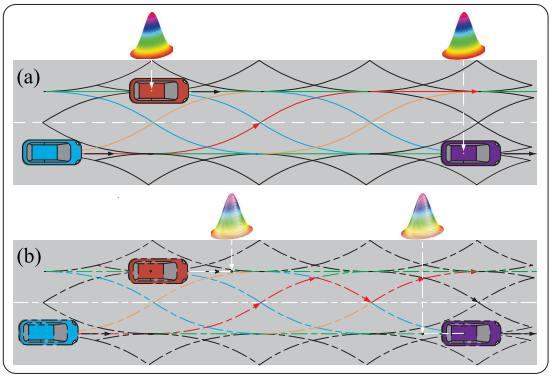

Fig. 10. Schematic of SpeedDown scenario.

speed difference between each obstacle and the ego vehicle, the corresponding offset distance is determined.

The schematic of a simple scenario is shown in Fig. 8, where the blue car is the ego vehicle and the red car and purple car are obstacles. The longitudinal velocities of the blue car, red car, and purple car are 50, 60, and 20 km/h, respectively. The BOAPF is generated by considering the velocity information to cope with the dynamic and time-varying surrounding environment. To further elaborate the principle, two typical scenarios are provided, as shown in Figs. 9 and 10.

The overtake scenario is shown in Fig. 9, where the primitive APF and BOAPF are shown in parts A and B, respectively. The red line in the sine grid denotes the planned path. The planned path in part A is generated according to the static surrounding environment, which indicates that the ego vehicle attempts to overtake along the planned path. The red dotted line in part B indicates that the ego vehicle still attempts to overtake along the same planned path after considering dynamic environment information. As a result, the ego vehicle overtakes along the planned path in this scenario.

The SpeenDown scenario is shown in Fig. 10, where the primitive APF is the same as the APF in Fig. 9(a). In this scenario, different from the overtake scenario, the ego vehicle attempts to change the lane at the beginning but gives up this maneuver by considering the velocity information finally. Specifically, the BOAPF changed due to the different longitudinal velocities of the red car, as shown in Fig. 10(b). In Fig. 10(a), the ego vehicle attempts to overtake along the red line, and however, the ego vehicle has a tendency to turn

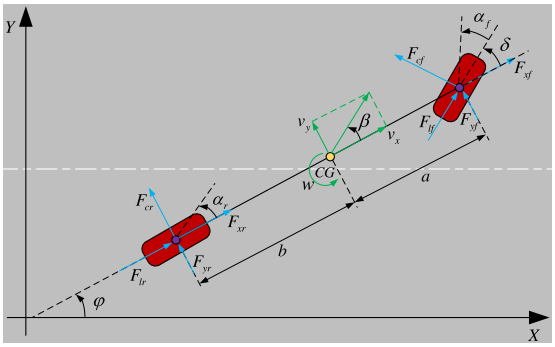

Fig. 11. Single-track model for vehicle.

in order to ensure collision-free after considering dynamic environment information, as shown in Fig. 10(b). It means that the conditions of overtaking are not satisfied. Consequently, the ego vehicle slows down instead of overtaking in this scenario.

Remark 4: We developed the classic APF [10] by taking the velocity information of the ego vehicle and obstacles into consideration to cope with the dynamic environment. As shown in Figs. 8–10, the feasible planned path for the ego vehicle can be generated based on the primitive potential field and BOAPF. By considering the velocity information and modifying the classic APF, the proposed approach can cope with the dynamic environment effectively.

Remark 5: The most critical information required in the proposed algorithm mainly includes the position (X_{Ego} and Y_{Ego}) and velocity V_{Ego} of the ego vehicle and the position (X_o and Y_o) and velocity V_o of obstacles, which are mainly used to predict of the dynamic environment and construct the TSPF. A large number of advanced devices and algorithms, including lidar, camera, and vehicle-to-everything (V2X) technology, are already available to collect the environmental information.

E. Motion Tracking Controller Design

The integrated motion planning and tracking framework [1], [28] is conducive to validating the planned path that is applicable to vehicle in practice and performance analysis. Thus, to illustrate the performance enhancement and track the planned smooth trajectory, the longitudinal and lateral motion tracking controllers based on MPC are designed in this section. The mathematical model of vehicle used in this article is the 3-DOF single-track model [29]–[31], as shown in Fig. 11, which takes the yaw motion, longitudinal motion and lateral motion of vehicle into consideration. The mass of the vehicle is 1720 kg, and the moment of inertia around the z-axis is 4170 kgm^2. The distances from center of gravity to front and rear wheel are 1.233 and 1.467 m, respectively. The half wheel track is 0.75 m. The cornering stiffness of front and rear tires is 1093 and 1167 N/deg, respectively. Define w, v_x, and v_y as yaw rate, longitudinal velocity, and lateral velocity of vehicle, respectively. The vehicle dynamics [32], which is generated by linearization, can be written as follows:

$$\dot{x} = Ax + Bu \tag{13}$$

$$y = Cx \tag{14}$$

$$x = \left[X \; v_x \; Y \; v_y \; \varphi \; w\right]^T \tag{15}$$

where A denotes the state matrix, B is the input matrix, C denotes the output matrix, $y = [Y\ \varphi]^T$, and $u = \delta$. The cost function can be written as follows:

$$J(x(t), \Delta U_t) = \sum_{i=1}^{N_p} \|\hat{y}_{t+i,t} - y_{\text{ref}t+i,t}\|_Q^2 + \sum_{i=0}^{N_c-1} \|\Delta u_{t+i,t}\|_R^2 \quad (16)$$

where N_c and N_p are the control horizon and the prediction horizon, respectively. The subscripts i and ref denote the ith instant and corresponding reference value, respectively. $\Delta U_t \triangleq [\Delta u_{t,t}, \ldots \Delta u_{t+N_c-1,t}]^T$ denotes the optimization vector, which is composed of control increment at time t. Moreover, Q and R indicate the weighting matrices for the corresponding terms, $\hat{y}_{t+i,t}$ represents the predicted output sequence at time $t+i$ obtained from $x_{t,t} = x(t)$ and $\Delta u_{t,t}, \ldots, \Delta u_{t+i,t}$. The finite-horizon optimal control problem can be solved online at time t as follows:

$$\min_{\Delta U_t} \ J(x(t), \Delta U_t) \quad (17)$$

$$\text{s.t. } x_{i+1,t} = \widetilde{A} x_{i,t} + \widetilde{B} \Delta u_{i,t} \quad (17a)$$

$$y_{i,t} = \widetilde{C} x_{i,t} \quad (17b)$$

$$y_{\min} \le y_{i,t} \le y_{\max} \quad (17c)$$

$$i = t, \ldots, t + N_p$$

$$u_{\min} \le u_{i,t} \le u_{\max} \quad (17d)$$

$$\Delta u_{\min} \le \Delta u_{i,t} \le \Delta u_{\max} \quad (17e)$$

$$u_{i,t} = u_{i-1,t} + \Delta u_{i,t}$$

$$i = t, \ldots, t + N_c - 1 \quad (17f)$$

where (17a) and (17b) are the discretized model (13) and (14) using the Euler method, (17c) denotes the constraints of the heading angle and the lateral location, and (17d) and (17e) denote the constraint of the control quantity. The principle of the longitudinal controller is similar to the lateral MPC controller. According to the current velocity and acceleration of the vehicle, the desired acceleration a_{des} can be obtained for generating the corresponding drive or brake to follow the planned velocity. The presented controllers can track the planned motion accurately and are utilized to verify the applicability of the proposed framework.

Remark 6: Parameter α_1 mainly affects the road potential field in the area between the road centerline and the road edge. α_2 mainly acts on the remaining areas of the road. The potential field value and the corresponding gradient of the area increase with bigger parameters. β mainly affects the magnitude of the potential field of the obstacle, while parameters γ_1 and γ_2 mainly affect the lateral and longitudinal action ranges of the potential field, respectively. λ can be chosen in (0 1.5], which mainly represents the effect of velocity information on the potential field distribution of the environment at future moments. Weight matrices Q and R denote the cost on the magnitudes of the tracking errors and control input, respectively. The relative size among weights is more important than the absolute size, reflecting the different relative cost distributions of the designed controller for the controlled input and different state tracking errors. Compared with the control horizon N_c, the prediction horizon N_p has a more important and obvious impact on the control performance. The prediction horizon N_p reflects how far ahead the model predicts the future system states. To a certain extent, increasing the prediction horizon N_p can make the control performance better, but it will increase the demand for computational resources. At the same time, when the prediction horizon N_p is too large, it also leads to the degradation of the control performance because the controller will consider more future trends of the system state. In this article, the weighting matrix $Q = [30\ 0;\ 0\ 280]$, $R = 1$, control horizon $N_c = 5$, and prediction horizon $N_p = 15$ for the lateral MPC controller. Meanwhile, $Q = 100$, $R = 0.01$, $N_c = 3$, and $N_p = 3$ for the longitudinal MPC controller. Note that the final control effect is the result of all parameters acting together and that these parameters can be further carefully adjusted according to the actual system response to obtain the desired control performance.

IV. Cosimulations and Analysis

In this section, the cosimulations of typical scenarios are provided to analyze the performance of the proposed new framework and prove the applicability. The proposed approach can be expanded to other scenarios with structured roads easily. The illustrative examples are cosimulated by using simulation platforms, where the proposed framework and algorithm are implemented in MATLAB/Simulink and the vehicle is modeled and parameterized in CarSim.

A. Performance Comparison With Classic APF

In order to further highlight the significance of the proposed SRN-based approach, the comparative simulations are performed in this section. The planned trajectories generated by different methods are provided and analyzed, including the classic APF (CPF) method [18], the SOTA resistance network-based (DRN) approach, and the proposed SRN algorithm. The superposed APF (TSPF) and the planned paths of CPF1 (goal attractive gain $k_p = 0.5$ and obstacle repulsive gain $\eta = 10$ [18]), CPF2 ($k_p = 0$ and $\eta = 10$), CPF3 ($k_p = 0.3$ and $\eta = 10$), CPF4 ($k_p = 1$ and $\eta = 10$) generated by the road APF (1), obstacle repulsive APF (2), and goal attractive APF [18] are shown in Fig. 12. Different from CPF1-4, the obstacle potential field and the corresponding repulsive force of CPF4 ($k_p = 1.5$ and $\eta = 20$) and CPF5 ($k_p = 2$ and $\eta = 10$) are obtained as detailed in [18] instead of (2). Meanwhile, the planned paths of DRN and SRN are also provided in Fig. 12.

The following useful conclusions can be drawn from the simulation results in Fig. 12.

1) The proposed SRN-based algorithm could overcome the local minimum problem efficiently. Note that CPF2 ($k_p = 0$ and $\eta = 10$) encounters local minimum without the goal attractive APF ($k_p = 0$). The goal APF [18] is unnecessary for the SRN-based approach and not constructed in this article. Once the virtual voltage source V_s is added, there must be a planned path generated based on the Kirchhoff circuit laws, which means that the local minimum does not exist.

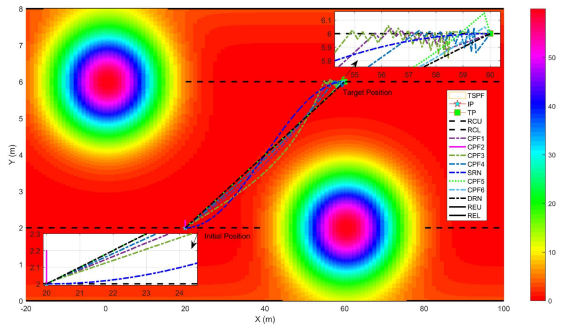

Fig. 12. Comparison of the planned trajectory. TSPF, IP, TP, RCU, RCL, REU, and REL denote the total superposed potential field, initial position (20, 2), target position (60, 6), upper road centerline, lower road centerline, upper road edge, and lower road edge, respectively.

2) The planned path is obtained from SRN based on current comparison [27] search rather than on the potential field gradient. The SRN is predesigned elaborately to ensure that the planned path is suitable for the autonomous electric vehicle.
3) The oscillation pheromone in the target point can be avoided with the constructed SRN, as shown in Fig. 12.

Remark 7: In terms of the principle of the algorithm, the APF is a motion planning method that requires less computational resources than algorithms such as RRT and lattice. The potential fields are used to reflect the surrounding environment in this article, which means that the planning approach proposed only requires the construction of an APF and does not require the calculation of the gradient of the potential field. Thus, the presented method can further optimize the computational complexity. The method for constructing the potential field and generating the planned paths based on the sinusoidal network has been given explicitly. It is clear that all the operations involved are simple addition, subtraction, multiplication, and division. Meanwhile, the algorithm was implemented using MATLAB 2016/Simulink and validated with the aid of the vehicle model in the high-field vehicle dynamics software CarSim 2016. The algorithm is deployed on a Win10 operating system with hardware configurations, including the Intel Core i7-10700 K CPU @3.80 GHz processor and 16.0-GB RAM. The time required for a single current generation is calculated to be about 0.00555 s, and it takes about 0.0044 s to generate the desired path based on the resistance network current by current comparison. The total simulation time is set to 10 s, and the actual running time of the cosimulation is about 2.4310 s with $N_c = 15$ and $N_p = 15$. The analysis and simulation results show that the computational complexity of the proposed motion planning method is feasible for practical applications. In the future, the algorithm can be further optimized by combining the advanced technologies, such as explicit MPC, parallel MPC, and MPC combined with other controllers [33]–[35].

B. Performance Comparison With SOTA Resistance Network Approach

This section based on the lane-change scenario compares the performance of the SOTA algorithm named DRN [17] with the proposed SRN. Cosimulation results in MATLAB/Simulink

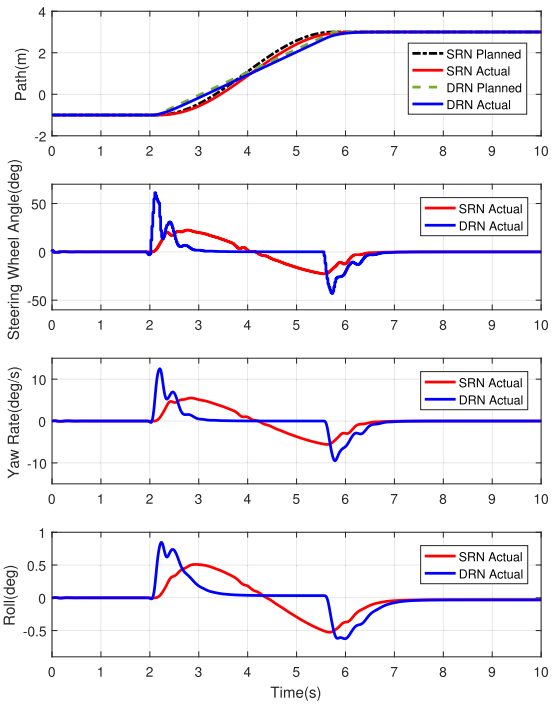

Fig. 13. Comparison of tracking performance.

and CarSim show the advantage of the proposed new framework.

To enhance the persuasiveness of the cosimulation results, the single variable method is utilized to carry out cosimulations. In the cosimulation, the same driver style is used in the SRN and DRN. Meanwhile, the same parameters of the controller are selected for SRN and DRN, and the velocity of the ego vehicle is set to 50 km/h. As shown in Fig. 13, the tracking performance of SRN and DRN is shown by the red and blue lines, respectively. Obviously, the planned path can be tracked by the proposed controller accurately.

To further analyze the performance capability of the ego vehicle, the steering wheel angle, yaw rate, and roll are shown in Fig. 13, in which the blue lines and red lines represent the dynamic change courses for DRN and SRN, respectively. As shown in Fig. 13, the steering wheel angle for DRN changes dramatically, and the amplitude of the DRN is about three times bigger than that of the SRN. It means that the planned continuous-curvature path for SRN contributes to tracking and improving the overall performance. By contrast, the dynamic change processes of the steering wheel angle for SRN are smoother and are more similar to the actual driving habit.

Especially, the smoother dynamic change process of the steering wheel angle results in a smoother yaw rate of the ego vehicle. Moreover, the roll reflects the vertical motion, which affects the drive comfort, and the more drastic roll angle change process denotes the more violent shake of the ego vehicle. As discussed above, SRN has a better performance capability in comparison to DRN in nature.

As summarized in Table I, the maximum and minimum steering wheel angle, yaw rate, and roll are listed to analyze the dynamic change courses quantitatively. Specifically, compared

TABLE I
COMPARISON OF MAXIMUM AND MINIMUM

Term(Unit)	Algorithm	Maximum	Minimum
Steering Wheel Angle(deg)	DRN	61.23	-43.06
	SRN	**20.52** (↓ 66.48%)	**-22.72** (↓ 47.23%)
Yaw Rate(deg/s)	DRN	12.47	-9.48
	SRN	**5.50** (↓ 55.89%)	**-5.58** (↓ 41.13%)
Roll(deg)	DRN	0.84	0.61
	SRN	**0.51** (↓ 39.28%)	**-0.52** (↓ 14.75%)

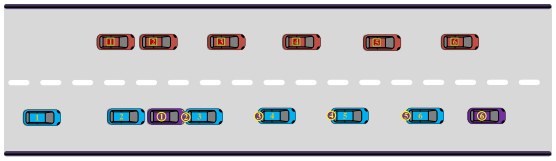

Fig. 14. SpeedDown scenario.

with DRN, the maximum steering wheel angle (more than 60%), yaw rate (more than 50%), and roll (about 40%) decrease significantly. Also, the minimum steering wheel angle (more than 45%), yaw rate (more than 40%), and roll (about 15%) decrease simultaneously. It further illustrates that the proposed new framework could make the ego vehicle run more smoothly and obtain better overall performance.

C. Scenarios Study

In this section, four representative scenarios are provided to illustrate the feasibility of the proposed new framework.

1) SpeedDown Scenario (S1): In this scenario, the target velocity of the ego vehicle is set to 50 km/h and the velocities of the vehicle in the adjacent lane and the front vehicle are set to 40 km/h. As shown in Fig. 14, the blue vehicle denotes the ego vehicle, the red vehicle and the purple vehicle represent the obstacles, and the different numbers denote the corresponding time of the vehicles.

According to the position and velocity information of the obstacles and the ego vehicle, the BOAPF is constructed to generate the planned motion, and then, the planned motion is tracked by the designed controller. The actual movement in this scenario is shown in Fig. 14, and the tracking performance and longitudinal velocity of the ego vehicle are shown in Fig. 15. Based on the dynamic surrounding information, the ego vehicle gives up changing lanes and slows down. The step-like planned speed is used to slow down for the ego vehicle. Some wonderful ideas of speed profile optimization can be found in [36] and [37], which is out of the scope of this article. As shown in Figs. 14 and 15, the collision-free motion can be generated and the planned motion can be tracked accurately with the proposed new framework.

2) Overtake Scenario (S2): In this scenario, the target velocity of the ego vehicle is set to 50 km/h, and the velocities of the vehicle in the adjacent lane and the front vehicle are set to 40 and 20 km/h, respectively. As shown in Fig. 16, the ego vehicle overtakes the front vehicle by changing the lane twice successfully along the planned collision-free path. Note that the corresponding states of the DRN approach are provided in the figures to compare the performance with the proposed SRN intuitively.

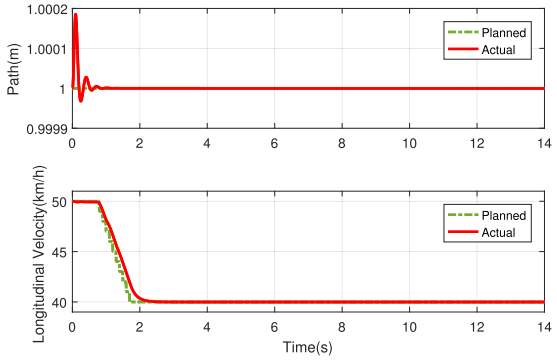

Fig. 15. Tracking performance and velocity information in S1.

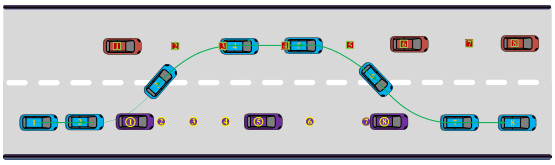

Fig. 16. Overtake scenario.

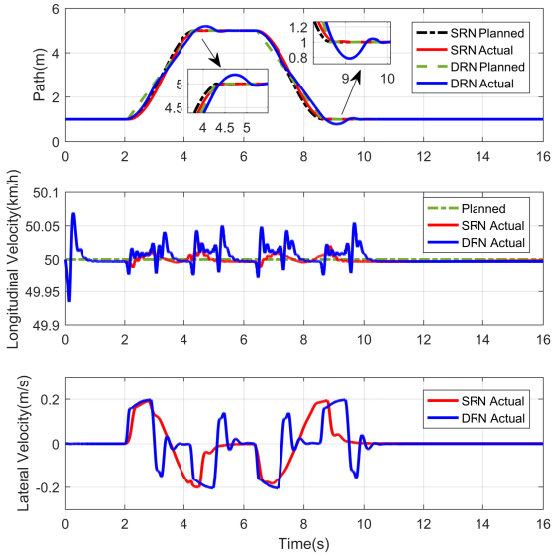

Fig. 17. Tracking performance and velocity information in S2.

As shown in Figs. 17 and 18, the longitudinal velocity of the ego vehicle keeps 50 km/h, the planned path can be tracked accurately, and the ego vehicle runs smoothly. More specifically, the current velocity of the ego vehicle is higher than that of the front vehicle. Thus, the ego vehicle must change the lane or slow down to ensure collision-free. The ego vehicle attempts to change the lane with the primitive APF, which is similar to Fig. 9(a). Meanwhile, like Fig. 9(b), the ego vehicle still tries to change into the adjacent lane with the constructed BOAPF by predicting the movement of other vehicles.

3) Complex Scenario (S3): To further testify the effectiveness of the proposed planning and tracking framework in dynamic environment, a more complex scenario is constructed in this section. The initial target velocity for the blue ego vehicle is set as 40 km/h; meanwhile, the velocities of the

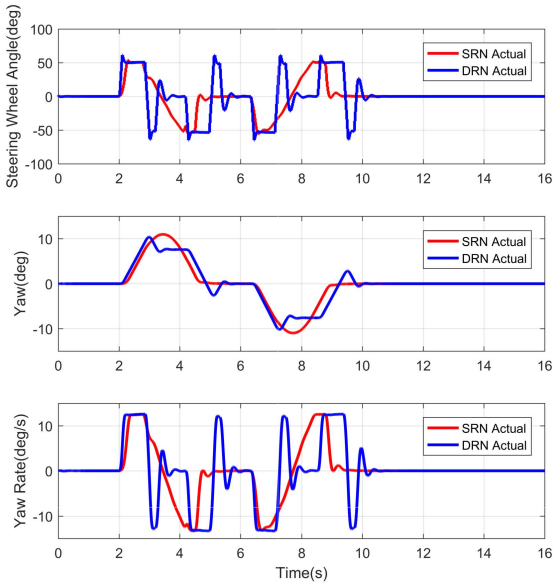

Fig. 18. Steer wheel and yaw information in S2.

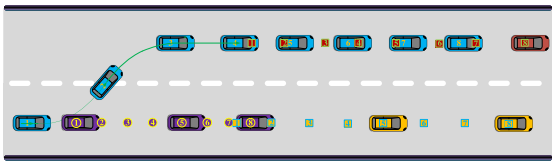

Fig. 19. Complex scenario.

obstacles are time-varying. The velocities of the purple vehicle, red vehicle, and yellow vehicle are $20 + \sin(2\pi * t)$, $30 + 2\sin(2\pi * t)$, and $30 + 2\sin(2\pi * t)$ km/h, respectively. As shown in Fig. 19, the ego vehicle changes into the adjacent lane and slows down to ensure collision-free.

Specifically, the ego vehicle changes into the adjacent lane by tracking the planned collision-free path, which is generated by the proposed novel SRN, as shown in Figs. 6 and 9. Then, the ego vehicle has to slow down to avoid collision, as shown in Fig. 19. The detailed information is shown in Figs. 20 and 21. The effectiveness of the proposed framework based on the novel SRN is proven by the full test of the different scenarios.

As shown in Fig. 19, the proposed novel SRN could generate a collision-free planned path according to the surrounding information. In comparison with the wonderful DRN approach, the proposed SRN generates a continuous-curvature planned path that contributes to tracking and improving overall performance. In particular, the steering wheel is turned back and forth for the DRN, while the steering wheel is turned smoothly for the SRN. Meanwhile, the dynamic process of the SRN is smoother than the DRN, and thus, the proposed SRN obtains better performance than the DRN obviously.

4) Emergent Braking Scenario (S4): In this scenario, the initial target velocity of the ego vehicle is set to 50 km/h, and the initial velocities of the front vehicle and the vehicle in the adjacent lane are also set to 50 km/h. However, the vehicle in the adjacent lane and the front vehicle stop suddenly. As detailed in Fig. 6, no path is feasible to overtake or change

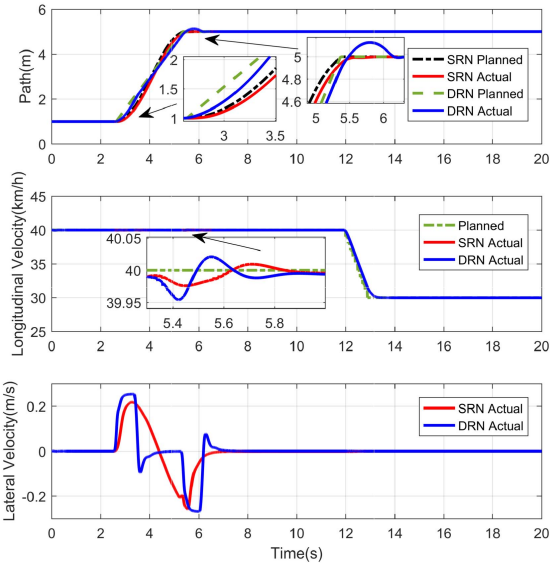

Fig. 20. Tracking performance and velocity information in S3.

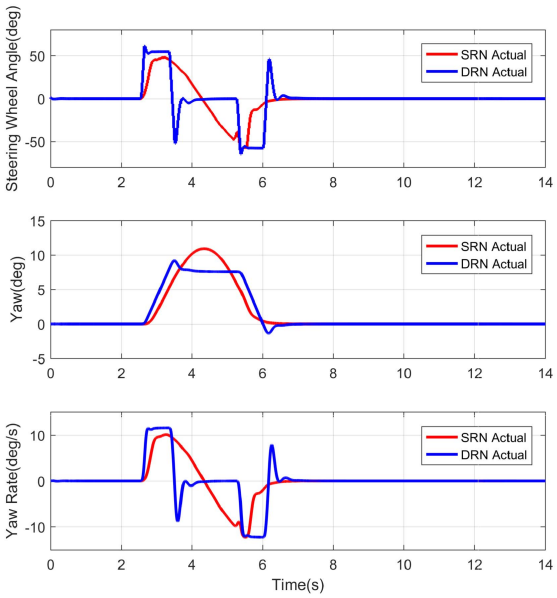

Fig. 21. Steer wheel and yaw information in S3.

lane, which causes the ego vehicle to brake emergently for avoiding collision. Specifically, in the initial stage, the purple vehicle in front, the red vehicle in the adjacent lane, and the blue ego vehicle travel at 50 km/h, but with the sudden stop of the vehicle in front and the vehicle in the adjacent lane, this vehicle brakes urgently for safety. As shown in Fig. 22, the vehicle can brake efficiently to avoid a collision and ensure vehicle safety. In detail, the velocity information, vehicle pitch angle denoted as red line, and longitudinal station denoted as blue line obtained from the high-fidelity simulation software CarSim are shown in Fig. 23. There are already some advanced technologies that can be introduced to further optimize the braking performance and safety of the system in the future, such as ABS [38] and AEB [39]. In general, the superiority and effectiveness of the proposed algorithm can be proved by

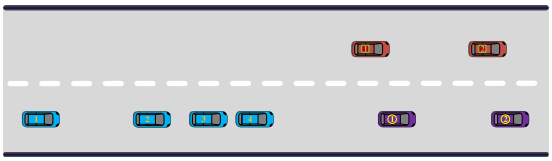

Fig. 22. Emergent braking scenario.

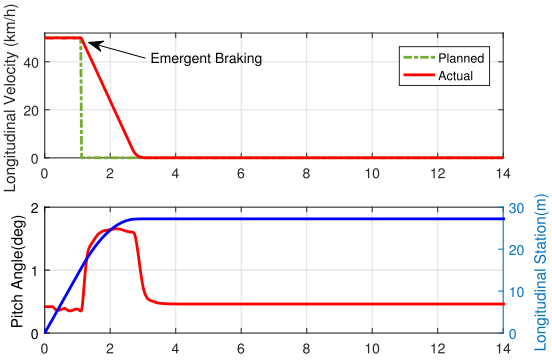

Fig. 23. Velocity information and braking performance in S4.

the scenarios study and comparative simulation results with the classic APF algorithm.

V. Conclusion

In this article, a new motion planning approach is proposed by improving the classical resistance network and APF method. The proposed SRN improves the planned path smoothness significantly, and the proposed BOAPF can cope with the dynamic environment by taking speed difference into consideration. In addition, we can choose different conservative coefficients or different SRN structures to select different driver styles. Cosimulation results in CarSim and MATLAB/Simulink is able to prove the advantage and effectiveness. Future work will attempt to verify the proposed approach on a real vehicle and extend this algorithm to curved road. Meanwhile, we will pay more attention to improving robustness [40] and fault tolerance to cope with more volatile and complicated scenarios by taking the sensor faults or actuator faults [41] into consideration.

References

[1] B. Paden, M. Čáp, S. Z. Yong, D. Yershov, and E. Frazzoli, "A survey of motion planning and control techniques for self-driving urban vehicles," *IEEE Trans. Intell. Veh.*, vol. 1, no. 1, pp. 33–55, Mar. 2016.

[2] K. P. Divakarla, A. Emadi, and S. Razavi, "A cognitive advanced driver assistance systems architecture for autonomous-capable electrified vehicles," *IEEE Trans. Transport. Electrific.*, vol. 5, no. 1, pp. 48–58, Mar. 2019.

[3] H. Pan and W. Sun, "Nonlinear output feedback finite-time control for vehicle active suspension systems," *IEEE Trans. Ind. Informat.*, vol. 15, no. 4, pp. 2073–2082, Apr. 2019.

[4] W. Sun, X. Wang, and C. Zhang, "A model-free control strategy for vehicle lateral stability with adaptive dynamic programming," *IEEE Trans. Ind. Electron.*, vol. 67, no. 12, pp. 10693–10701, Dec. 2020.

[5] C. Liu, W. Zhan, and M. Tomizuka, "Speed profile planning in dynamic environments via temporal optimization," in *Proc. IEEE Intell. Vehicles Symp. (IV)*, Jun. 2017, pp. 154–159.

[6] U. Lee, S. Yoon, H. Shim, P. Vasseur, and C. Demonceaux, "Local path planning in a complex environment for self-driving car," in *Proc. 4th Annu. IEEE Int. Conf. Cyber Technol. Autom., Control Intell.*, Jun. 2014, pp. 445–450.

[7] S. J. Anderson, S. B. Karumanchi, and K. Iagnemma, "Constraint-based planning and control for safe, semi-autonomous operation of vehicles," in *Proc. IEEE Intell. Vehicles Symp.*, Jun. 2012, pp. 383–388.

[8] M. Montemerlo *et al.*, "Junior: The Stanford entry in the urban challenge," *J. Field Robot.*, vol. 25, no. 9, pp. 569–597, 2008.

[9] Z. Liu, S. Pang, S. Gong, and P. Yang, "Robot path planning in impedance networks," in *Proc. 6th World Congr. Intell. Control Autom.*, Jun. 2006, pp. 9109–9113.

[10] M. Gyu Park, J. Hyun Jeon, and M. Cheol Lee, "Obstacle avoidance for mobile robots using artificial potential field approach with simulated annealing," in *Proc. IEEE Int. Symp. Ind. Electron. (ISIE)*, Jun. 2001, pp. 1530–1535.

[11] M. B. Oetiker, G. P. Baker, and L. Guzzella, "A navigation-field-based semi-autonomous nonholonomic vehicle-parking assistant," *IEEE Trans. Veh. Technol.*, vol. 58, no. 3, pp. 1106–1118, Mar. 2009.

[12] T. Tsuji, Y. Tanaka, P. G. Morasso, V. Sanguineti, and M. Kaneko, "Bio-mimetic trajectory generation of robots via artificial potential field with time base generator," *IEEE Trans. Syst., Man, C, Appl. Rev.*, vol. 32, no. 4, pp. 426–439, Nov. 2002.

[13] M. Bojarski *et al.*, "End to end learning for self-driving cars," 2016, *arXiv:1604.07316*.

[14] C. You, J. Lu, D. Filev, and P. Tsiotras, "Autonomous planning and control for intelligent vehicles in traffic," *IEEE Trans. Intell. Transp. Syst.*, vol. 21, no. 6, pp. 2339–2349, Jun. 2020.

[15] J. Nilsson, M. Brännström, J. Fredriksson, and E. Coelingh, "Longitudinal and lateral control for automated yielding maneuvers," *IEEE Trans. Intell. Transp. Syst.*, vol. 17, no. 5, pp. 1404–1414, May 2016.

[16] J. Chen, W. Zhan, and M. Tomizuka, "Autonomous driving motion planning with constrained iterative LQR," *IEEE Trans. Intell. Veh.*, vol. 4, no. 2, pp. 244–254, Jun. 2019.

[17] Y. Huang, H. Wang, A. Khajepour, H. Ding, K. Yuan, and Y. Qin, "A novel local motion planning framework for autonomous vehicles based on resistance network and model predictive control," *IEEE Trans. Veh. Technol.*, vol. 69, no. 1, pp. 55–66, Jan. 2020.

[18] O. Khatib, "Real-time obstacle avoidance for manipulators and mobile robots," *Int. J. Robot. Res.*, vol. 5, no. 1, pp. 90–98, 1986, doi: 10.1177/027836498600500106.

[19] H.-T. Chiang, N. Malone, K. Lesser, M. Oishi, and L. Tapia, "Path-guided artificial potential fields with stochastic reachable sets for motion planning in highly dynamic environments," in *Proc. IEEE Int. Conf. Robot. Autom. (ICRA)*, May 2015, pp. 2347–2354.

[20] G. Li, Y. Tamura, A. Yamashita, and H. Asama, "Effective improved artificial potential field-based regression search method for autonomous mobile robot path planning," *Int. J. Mechatron. Autom.*, vol. 3, no. 3, pp. 141–170, 2013.

[21] N. Malone, H.-T. Chiang, K. Lesser, M. Oishi, and L. Tapia, "Hybrid dynamic moving obstacle avoidance using a stochastic reachable set-based potential field," *IEEE Trans. Robot.*, vol. 33, no. 5, pp. 1124–1138, Oct. 2017.

[22] F. Bayat, S. Najafinia, and M. Aliyari, "Mobile robots path planning: Electrostatic potential field approach," *Expert Syst. Appl.*, vol. 100, pp. 68–78, Jun. 2018.

[23] T. Bonny and M. Kashkash, "Highly optimized Q-learning-based bees approach for mobile robot path planning in static and dynamic environments," *J. Field Robot.*, pp. 1–18, 2021, doi: 10.1002/rob.22052.

[24] N. H. Amer, H. Zamzuri, K. Hudha, and Z. A. Kadir, "Modelling and control strategies in path tracking control for autonomous ground vehicles: A review of state of the art and challenges," *J. Intell. Robot. Syst.*, vol. 86, no. 2, pp. 225–254, May 2017.

[25] L. Zhang, Z. Zhang, Z. Wang, J. Deng, and D. G. Dorrell, "Chassis coordinated control for full X-by-wire vehicles—A review," *Chin. J. Mech. Eng.*, vol. 34, no. 1, pp. 1–25, Dec. 2021.

[26] S. Waydo and R. M. Murray, "Vehicle motion planning using stream functions," in *Proc. IEEE Int. Conf. Robot. Autom.*, Sep. 2003, pp. 2484–2491.

[27] G.-X. Cheng, M. Ikegami, and M. Tanaka, "A resistive mesh analysis method for parallel path searching," in *Proc. 34th Midwest Symp. Circuits Syst.*, May 1992, pp. 827–830.

[28] K. Berntorp, R. Bai, K. F. Erliksson, C. Danielson, A. Weiss, and S. D. Cairano, "Positive invariant sets for safe integrated vehicle motion planning and control," *IEEE Trans. Intell. Vehicles*, vol. 5, no. 1, pp. 112–126, Mar. 2020.

[29] N. Guo, X. Zhang, Y. Zou, B. Lenzo, and T. Zhang, "A computationally efficient path-following control strategy of autonomous electric vehicles with yaw motion stabilization," *IEEE Trans. Transport. Electrific.*, vol. 6, no. 2, pp. 728–739, Jun. 2020.

[30] N. Guo, X. Zhang, Y. Zou, B. Lenzo, G. Du, and T. Zhang, "A supervisory control strategy of distributed drive electric vehicles for coordinating handling, lateral stability, and energy efficiency," *IEEE Trans. Transport. Electrific.*, vol. 7, no. 4, pp. 2488–2504, Dec. 2021.
[31] L. Guo, B. Yang, J. Ye, J. M. Velni, and W. Song, "Attack-resilient lateral stability control for four-wheel-driven EVs considering changed driver behavior under cyber threats," *IEEE Trans. Transport. Electrific.*, early access, Aug. 3, 2021, doi: 10.1109/TTE.2021.3102134.
[32] F. Borrelli, P. Falcone, T. Keviczky, J. Asgari, and D. Hrovat, "MPC-based approach to active steering for autonomous vehicle systems," *Int. J. Vehicle Auto. Syst.*, vol. 3, nos. 2–4, pp. 265–291, Jan. 2005.
[33] Y. M. Mok, L. Zhai, C. Wang, X. Zhang, and Y. Hou, "A post impact stability control for four hub-motor independent-drive electric vehicles," *IEEE Trans. Veh. Technol.*, vol. 71, no. 2, pp. 1384–1396, Feb. 2022.
[34] J. Zhu, Z. Wang, L. Zhang, and D. G. Dorrell, "Braking/steering coordination control for in-wheel motor drive electric vehicles based on nonlinear model predictive control," *Mechanism Mach. Theory*, vol. 142, Dec. 2019, Art. no. 103586.
[35] D. Liu, J. Wang, and S. Wang, "Coordinated motion control and event-based obstacle-crossing for four wheel-leg independent motor-driven robotic system," *Mechatronics*, vol. 81, Feb. 2022, Art. no. 102697.
[36] Y. Wang, J.-R. Chardonnet, and F. Merienne, "Speed profile optimization for enhanced passenger comfort: An optimal control approach," in *Proc. 21st Int. Conf. Intell. Transp. Syst. (ITSC)*, Nov. 2018, pp. 723–728.
[37] D. Gonzalez, V. Milanes, J. Perez, and F. Nashashibi, "Speed profile generation based on quintic Bézier curves for enhanced passenger comfort," in *Proc. IEEE 19th Int. Conf. Intell. Transp. Syst. (ITSC)*, Nov. 2016, pp. 814–819.
[38] L. Zhang, L. Yu, N. Pan, Y. Zhang, and J. Song, "Cooperative control of regenerative braking and friction braking in the transient process of anti-lock braking activation in electric vehicles," *Proc. Inst. Mech. Eng., D, J. Automobile Eng.*, vol. 230, no. 11, pp. 1459–1476, Sep. 2016.
[39] N. Kaempchen, B. Schiele, and K. Dietmayer, "Situation assessment of an autonomous emergency brake for arbitrary vehicle-to-vehicle collision scenarios," *IEEE Trans. Intell. Transp. Syst.*, vol. 10, no. 4, pp. 678–687, Dec. 2009.
[40] Z. Liu and H. Pan, "Barrier function-based adaptive sliding mode control for application to vehicle suspensions," *IEEE Trans. Transport. Electrific.*, vol. 7, no. 3, pp. 2023–2033, Sep. 2021.
[41] H. Pan, H. Li, W. Sun, and Z. Wang, "Adaptive fault-tolerant compensation control and its application to nonlinear suspension systems," *IEEE Trans. Syst., Man, Cybern. Syst.*, vol. 50, no. 5, pp. 1766–1776, May 2020.

Tenglong Huang received the B.E. degree in automation from the Henan University of Technology, Zhengzhou, China, in 2019, where he is currently pursuing the Ph.D. degree with the Research Institute of Intelligent Control and Systems, Harbin Institute of Technology, Harbin, China.

His current research interests include motion planning, vehicle dynamics control, adaptive control, and fault-tolerant control.

Huihui Pan received the Ph.D. degree in control science and engineering from the Harbin Institute of Technology, Harbin, China, in 2017, and the Ph.D. degree in mechanical engineering from The Hong Kong Polytechnic University, Hong Kong, in 2018.

Since December 2017, he has been with the Research Institute of Intelligent Control and Systems, Harbin Institute of Technology. His research interests include nonlinear control, vehicle dynamic control, and intelligent vehicles.

Dr. Pan is an Associate Editor of IEEE TRANSACTIONS ON INTELLIGENT VEHICLES and *Mechatronics*.

Weichao Sun (Senior Member, IEEE) received the Ph.D. degree in control science and engineering from the Harbin Institute of Technology, Harbin, China, in 2013.

He is currently a Professor with the Research Institute of Intelligent Control Systems, Harbin Institute of Technology. His research interests include adaptive robust control, mechatronics, robotics, and autonomous vehicles.

Dr. Sun is an Associate Editor for IEEE TRANSACTIONS ON SYSTEMS, MAN, AND CYBERNETICS: SYSTEMS, *Mechatronics*, and *Journal of Dynamic Systems, Measurement and Control*.

Huijun Gao (Fellow, IEEE) received the Ph.D. degree in control science and engineering from the Harbin Institute of Technology, Harbin, China, in 2005.

From 2005 to 2007, he carried out his post-doctoral research with the Department of Electrical and Computer Engineering, University of Alberta, Edmonton, AB, Canada. Since 2004, he has been with the Harbin Institute of Technology, where he is currently a Chair Professor and the Director of the Research Institute of Intelligent Control and Systems. His research interests include intelligent and robust control, robotics, mechatronics, and their engineering applications.

Dr. Gao is a member of Academia Europaea and a Distinguished Lecturer of the IEEE Systems, Man and Cybernetics Society. He is the Vice President of the IEEE Industrial Electronics Society and a Council Member of the International Federation of Automatic Control (IFAC). He serves/served as the Editor-in-Chief of the IEEE/ASME TRANSACTIONS ON MECHATRONICS, the Co-Editor-in-Chief for the IEEE TRANSACTIONS ON INDUSTRIAL ELECTRONICS, and an Associate Editor of *Automatica*, the IEEE TRANSACTIONS ON CYBERNETICS, and the IEEE TRANSACTIONS ON INDUSTRIAL INFORMATICS.